Bioactive Materials 6 (2021) 91–105

Contents lists available at ScienceDirect

Bioactive Materials

journal homepage: http://www.keaipublishing.com/biomat

Osteogenesis, angiogenesis and immune response of Mg-Al layered double hydroxide coating on pure Mg

Shi Cheng[a,b], Dongdong Zhang[c], Mei Li[a], Xuanyong Liu[c,d], Yu Zhang[a,*], Shi Qian[c,d,**], Feng Peng[a,***]

[a] Department of Orthopedics, Guangdong Provincial People's Hospital, Guangdong Academy of Medical Sciences, Guangzhou, Guangdong, 510080, China
[b] The Second School of Clinical Medicine, Southern Medical University, Guangzhou, 510515, China
[c] State Key Laboratory of High Performance Ceramics and Superfine Microstructure, Shanghai Institute of Ceramics, Chinese Academy of Sciences, Shanghai, 200050, China
[d] Cixi Center of Biomaterials Surface Engineering, Shanghai Institute of Ceramics, Chinese Academy of Sciences, Ningbo, 315300, China

ARTICLE INFO

Keywords:
Magnesium
Layered double hydroxide
Osteogenesis
Angiogenesis
Immune response

ABSTRACT

Layered double hydroxides (LDHs) are widely studied to enhance corrosion resistance and biocompatibility of Mg alloys, which are promising bone implants. However, the influence of LDH coating on the osteointegration of Mg implants lacks of a systematic study. In this work, Mg-Al LDH coating was prepared on pure Mg via hydrothermal treatment. The as-prepared Mg-Al LDH coated Mg exhibited better *in vitro* and *in vivo* corrosion resistance than bare Mg and $Mg(OH)_2$ coated Mg. *In vitro* culture of mouse osteoblast cell line (MC3T3-E1) suggested that Mg-Al LDH coated Mg was more favorable for its osteogenic differentiation. *In vitro* culture of HUVECs revealed that cells cultured in the extract of Mg-Al LDH coated Mg showed superior angiogenic behaviors. More importantly, the immune response of Mg-Al LDH coated Mg was studied by *in vitro* culturing murine-derived macrophage cell line (RAW264.7). The results verified that Mg-Al LDH coated Mg could induce macrophage polarize to M2 phenotype (anti-inflammatory). Furthermore, the secreted factor in the macrophage-conditioned culture medium of Mg-Al LDH group was more suitable for the bone differentiation of rat bone marrow stem cells (rBMSCs) and the angiogenic behavior of human umbilical vein endothelial cells (HUVECs). Finally, the result of femoral implantation suggested that Mg-Al LDH coated Mg exhibited better osteointegration than bare Mg and $Mg(OH)_2$ coated Mg. With favorable *in vitro* and *in vivo* performances, Mg-Al LDH is promising as protective coating on Mg for orthopedic applications.

1. Introduction

With biodegradability and proper mechanical properties, Magnesium (Mg) and its alloys are attracting increasing attention in the field of metal-based biomaterials, especially for orthopedic applications [1–3]. Under the unremitting efforts of researchers, Mg based products were available on the market since several years ago. In 2013, Mg-based products, including screw and bone nail et al., of Syntellix Company were certified by Conformite Europeenne (CE) [4]. Subsequently, in 2015, Mg-Ca alloy screw of U&I Company was approved by Korea Food and Drug Administration (KFDA) [5]. Currently, numerous Mg-based implants have carried out or is about to carry out clinical trial [6]. Though the above *in vitro* and *in vivo* investigations have proved the security and potential application of Mg-based implants, there are limitations in the large scale of application. For example, its fast degradation would cause huge damage to its mechanical integrity and accumulation of hydrogen [7–9]. Therefore, Mg-based implants with highly desirable corrosion resistance are urgent to be designed and fabricated.

One of the effective methods to enhance the corrosion resistance of Mg-based implants is alloying. Many elements are added to Mg substrate to develop various types of Mg alloys, such as Mg-Ca, Mg-Sr, Mg-Li and Mg-Zn-Ca [10–12]. However, the fast degradation in the initial period of implantation is inevitable, because the intrinsic low standard

Peer review under responsibility of KeAi Communications Co., Ltd.
* Corresponding author.
** Corresponding author. State Key Laboratory of High Performance Ceramics and Superfine Microstructure, Shanghai Institute of Ceramics, Chinese Academy of Sciences, Shanghai, 200050, China.
*** Corresponding author.
E-mail addresses: luck_2001@126.com (Y. Zhang), qianshi@mail.sic.ac.cn (S. Qian), peng_feng7@163.com (F. Peng).

https://doi.org/10.1016/j.bioactmat.2020.07.014
Received 9 June 2020; Received in revised form 21 July 2020; Accepted 21 July 2020

potential of Mg (−2.37 V vs NHE) [13]. Another choice is surface modification, such as plasma electrolytic oxidation, spray coating, hydrofluoric acid treatment, hydrothermal treatment and plasma ion immersion implantation [14–18]. Among these films, layered double hydroxide (LDH) have been extensively studied for its biodegradation and unique structure, as well as favorable corrosion protection [19,20]. LDH is composed of positive charged hydroxide layer and negative charged interlayer, and its molecular formula is $[M^{2+}_{1-x}M^{3+}x(OH)_2][A^{n-}]_{x/n}{\cdot}zH2O$, where M^{2+} means bivalent cations and M^{3+} means trivalent cations [21,22].

Among various kinds of LDH coatings on Mg alloy, Mg-Al LDH is most studied for its easiest synthetization. In previous studies, Mg-Al LDH coatings were prepared on Mg alloy via different methods (such as hydrothermal treatment and steam coating), and all these results suggested that Mg-Al LDH coatings showed enhanced corrosion resistance and biocompatibility [23–25]. Though *in vitro* corrosion resistance and biocompatibility of Mg-AL LDH coating on Mg alloy has been widely explored, there lacks of a systematic study of the response of osteogenesis-related cells to Mg-Al LDH coating, as well as a systematic study of *in vivo* performance of Mg-Al LDH coating.

In the present study, we fabricated a Mg-Al LDH coating on pure Mg via hydrothermal treatment. We first evaluated the influence of Mg-Al LDH coating on the differentiation of mouse osteoblast cell line MC3T3-E1. Beyond that, good osteointegration is always accompanied with fast vascular formation, because the growth of new bone needs the nutrients supplied by the vessel [26–28]. Hence, we then detected the influence of Mg-Al LDH coating on the angiogenic behavior of human umbilical vein endothelial cells (HUVECs). Furthermore, the implantation of foreign body material will induce immune response, especially at the initial 3-7 days. Macrophage plays an important role in immune response and will be activated to M1 phenotype (pro-inflammatory) or M2 phenotype (anti-inflammatory). Macrophage in M2 phenotype will secret a large number of anti-inflammatory cytokines and growth factors to promote the growth of new bone [29–31]. Therefore, the immune response induced by Mg-Al LDH coated Mg was studied by culturing murine-derived macrophage cell line RAW264.7. In addition, the influence of cytokines and growth factors secreted by RAW264.7 on rat bone marrow stem cells (rBMSCs) and HUVECs behaviors were also investigated. Finally, the corrosion resistance/immune response, and osteointegration capability of Mg-Al LDH coated Mg were studied by subcutaneous implantation and femur implantation, respectively.

2. Materials and methods

2.1. Sample preparation and characterization

Pure Mg (> 99.9%) plates were cut into sheets with 10 mm × 10 mm × 2 mm (for *in vitro* tests and subcutaneous implantation) and rods with a diameter of 2 mm, length of 10 mm (for femoral implantation). The cut sheets were ground with 1000# SiC paper to remove oxide layer and contaminant, as well as get a relatively smooth surface. Then the cut rods and the ground substrates were ultrasonically cleaned in ethanol, and dry with a blow drier before utilization.

Mg sheets and rods were placed in a Teflon-line stainless. To prepare $Mg(OH)_2$ film, 50 mL ultrapure water added with 400 μL NaOH (10 M) was gently pour into the Teflon-line. To prepare LDH film, 50 mL Al $(NO_3)_3$ (0.02 M) added with 600 μL NaOH (10 M) was gently pour into the Teflon-line stainless. Both the reaction kettles were kept at 120 °C. After 12 h, the samples were taken out, ultrasonically cleaned for 5 min and rinsed with deionized water. The obtained samples were denoted as Mg-$Mg(OH)_2$ and Mg-LDH, respectively.

Scanning electron microscopy (SEM; Hitachi-S3400 N, Hitachi, Japan) was used to observe the surface morphologies of Mg, Mg-Mg $(OH)_2$ and Mg-LDH samples, and corresponding element compositions were evaluated by energy dispersive spectrometry (EDS; IXRF-550i, IXRF SYSTEMS, USA). X-ray diffraction analysis of all the samples was applied on a TTR-Z diffractometer (Rigaku, Japanese) with Cu Ka radiation.

2.2. In vitro corrosion evaluation

Electrochemical analyses were conducted in phosphate buffer saline (PBS) via an electrochemical analyzer (CHI760C, Shanghai, China) according to the previous study [32]. Briefly, a three-electrode cell was employed with the sample as working electrode (0.255 cm^2), a graphite rod as counter electrode and a saturated calomel electrode (SCE) as reference electrode. Prior to the tests, the samples were stabilized in PBS. The potentiodynamic polarization (PDP) test was performed at a constant voltage scan rate of 10 mV/s. Tafel extrapolation was used to calculate the values of corrosion potential (E_{corr}), current density (j_{corr}) and corrosion resistance (R_p). Electrochemical impedance spectroscopy (EIS) measurements were performed with a perturbation signal of 5 mV and recorded from 10^5 Hz to 10^{-2} Hz. The EIS results were fitted via ZView software.

Hydrogen evolution test was conducted by a self-made set up. In details, Mg, Mg-$Mg(OH)_2$ and Mg-LDH samples were placed in beakers with 360 mL PBS (four specimens of each group in one beak). The samples were covered by funnels and kept in a water bath at 37 °C. The released hydrogen was recorded every day for 10 days.

2.3. Cell culture and preparation of materials' extract

HUVECs, MC3T3-E1, rBMSCs and RAW264.7 were involved in this study. All of the cells were purchased from American Type Culture Collection (ATCC). MC3T3-E1 and rBSMCs were cultured in α-MEM supply with 10% Fetal bovine serum (FBS, Gibco, Tauranga, New Zealand) and 1% penicillin and streptomycin (P/S); HUVECs was cultured in Endothelial Cell Medium (Sciencell, USA) supply with 10% FBS, 1% P/S, and 1% endothelial cell growth supplement/heparin kit (ECGS/H, Sciencell, USA); RAW264.7 was cultured in the dulbecco's modified eagle media: nutrient mixture F-12 (DMEM/F12, Hyclone), supplemented with 10% fetal bovine serum and 1% P/S. Cells were cultured at 37 °C in a humidified atmosphere of 5% CO_2 and 95% air, and sub-cultured when they were reached to 80%–90% confluence. Cells at passage 3-5 were used in this study.

Sample plates were immersed in completed culture medium mentioned above at cell culture conditions of 37 °C, 5% CO_2, and 95% humidity for 1 day to obtain the extracts. The specimen area to solution volume ratio was 1.25 cm^2/mL, which was determined by ISO 10993-5 [33]. Acquired extracts of each sample were subsequently used for the following *in vitro* cell experiments.

2.4. Cell viability detection

MC3T3-E1 or HUVECs were seeded at 1 × 10^4 cells/mL in 96-well plates. After 1 day for complete cell attachment, the growth medium was discarded and replaced with sample extracts. Then they were further incubated for 1, 3, 5 and 7 days. At each time point, Cell Counting Kit-8 (CCK-8; Dojindo Molecular Technology, Japan) assay was used to evaluate the number of viable cells. After reaction with mixed working solution for 2.5 h, the optical density (OD) of each well was measured at 450 nm using a microplate reader (Bio-Tek, USA).

2.5. In vitro osteogenic differentiation of MC3T3-E1

2.5.1. Extracellular matrix mineralization assay

Alizarin Red S (SigmaAldrich, USA) staining was used to detect the degree of extracellular matrix mineralization (ECM). In brief, MC3T3-E1 were seeded at 1 × 10^5 cells/mL in 24-well plates and cultured with sample extracts supplied with 10 mM β-glycerophosphate, 100 nM dexamethasone, 50 mM ascorbate and glutamine. After osteogenic

induction for 7 days, the cells were fixed with 4% paraformaldehyde for 30 min followed by staining with Alizarin Red S for 30 min at room temperature. After rinsed with PBS to eliminate non-specific staining, images were captured under a phase contrast inverted optics microscope (Olympus, Germany). Thereafter, to semi-quantitative analysis of mineralized extracellular matrix, mineralized nodules were dissolved with 10% cetylpyridinium chloride (SigmaAldrich, USA) and measured the absorbance at 620 nm.

2.5.2. Alkaline phosphatase (ALP) activity assay

The intracellular ALP activity was evaluated qualitatively and quantitatively. In the qualitative assay, cells after osteogenic induction for 7 days with medium mentioned above were washed with PBS and fixed by 4% paraformaldehyde. Then they were stained with BCIP/NBT ALP Color Development Kit (Beyotime, China) according to the manufacturer's instructions. Alkaline Phosphatase Assay Kit (Beyotime, China) was adopted to quantitatively test the ALP activity at day 3 and day 7. Briefly, cells were lysed in RIPA (P0013J, Beyotime, China) to extract total proteins, then the protein content were determined by the bicinchoninic acid (BCA) Protein Assay Kit (Beyotime, China). Afterwards, ALP activity was quantified based on the conversion of colorless p-nitrophenyl phosphate (pNPP) to colored p-nitrophenol after co-incubation for 30 min at 37 °C. The results were exhibited as U per ng of total protein.

2.5.3. Quantitative real time-polymerase chain reaction (qRT-PCR)

MC3T3-E1 were seeded at 2×10^5 cells/mL on 12 well plates for 1 day, then the medium was replaced with sample extracts and continue to culture for 3–7 days. The expression of osteogenic genes such as bone morphology protein-2 (BMP-2), Collagen-I (Col-I), ALP, and osteocalcin (OCN), were evaluated by qRT-PCR. Briefly, total RNA was extracted according to Trizol (SigmaAldrich, USA) method and quantified by nanodrop 2000 (Thermofisher, USA). Then 1 μg total RNA was reversely transcribed into cDNA using the 1st Strand cDNA synthesis supermix Kit (Yeasen, China). Synthesized cDNA was then mixed with SYBR Green Mastermix and primers to quantify the gene expression of the target genes. Genes were analyzed using GAPDH as a housekeeping gene, and $2^{-\triangle\triangle CT}$ method was used for normalization and relative quantification. The primer sequences are listed in Table S1.

2.6. In vitro angiogenic differentiation of HUVECs

2.7.1. Tube formation assay

Tube formation assay, a classic angiogenesis assay based on the angiogenic differentiation of endothelial cells, was selected in our study to exam the angiogenic effect on HUVECs of each sample. One day before experiment, pipets, 24-well culture plates and sterile tips were cooled in −20 °C. Then thaw the Matrigel (BD Matrigel™356234, USA) at 4 °C, keep all the procedure on ice. Coated 24-well plates with 300 μL per well of Matrigel and warmed in 37 °C incubator for 15 min to allow gelling of the Matrigel. Added 4×10^6 HUVECs within 1 mL of sample extracts into each cell, further cultured for 4 h. Then observe the tube structures under a phase contrast inverted microscope (Olympus, Germany). Total branch length was analyzed by image J software with Angiogenesis Analyzer plug.

2.7.2. qRT-PCR

HUVECs were seeded at 2×10^5 cells/mL on 12 well plates for 1 day, then the medium was replaced with sample extracts and continue to culture for 3 and 7 days. At each time points, total RNA was extracted for qRT-PCR, the experiment procedure has been described in 2.5.3. The expression of classic angiogenic related genes, such as vascular endothelial growth factor (VEGF), vascular endothelial growth factor receptor 2 (KDR) and hypoxia-inducible factor 1-alpha (HIF-1α), were analyzed. The primer sequences are listed in Table S2.

2.8. Proliferation and polarization of macrophages

RAW264.7 were seeded at 5×10^3 cells/mL in 96-well plates. After 1 day for complete cell attachment, the growth medium was discarded and replaced with sample extracts. Then they were further incubated for 1 and 3 days. At each time point, CCK-8 assay was used to evaluate the number of viable cells as mentioned 2.4.

RAW264.7 were seeded at 5×10^5 cells/mL in 6-well plates. After culturing for 3 days, the expression of M1 (Interleukin-1 (IL-1), Tumor necrosis factor-α (TNF-α), and Chemokine ligand-2 (CCL-2)) and M2 (Interleukin −10 (IL-10), CD163, and Chemokine ligand-22 (CCL-22))) related genes were detected by qRT-PCR technology as mentioned in 2.5.3. The involved primer sequences are listed in Table S3.

2.9. Effects of macrophage-conditioned culture medium on rBMSCs

2.9.1. The preparation of macrophage-conditioned culture medium (MCM)

RAW264.7 were seeded at 5×10^5 cells/mL in 6-well plates. After culturing for 1 day, the culture medium was removed and added with material's extracts. To avoid the influence of pH value and Mg ions concentration, the extracts were removed after culturing for 3 days and added with fresh DMEMF12. After culturing for 2 day, the supernatants were collected and centrifugated at 1000 rpm for 5 min. The obtained supernatants were denoted as MCM.

2.9.2. Immunofluorescence staining and qRT-PCR

rBMSC were seeded at 2×10^5 cells/mL in 6-well plates. The culture medium was replaced by MCM after culturing for 1 day. The MCM were refreshed after culturing for another 4 days. At day 7 after cultured in MCM, cells were rinsed by PBS, and fixed in 4% paraformaldehyde (PFA). After that, cells were permeabilized in 0.1 v/v % Triton X-100, blocked with 10% bovine serum albumin, and cultured with the primary antibodies of anti-COL-I (Abcam, ab76956). Then, goat anti-mouse IgG second ary antibody (Abcam, ab150115) were added to conjugate fluorescein isothiocyanate. Afterwards, nucleus was stained with DAPI. Runt-related transcription factor-2 (RUNX-2) was also stained as mentioned above. A fluorescence microscope was applied to observe the stained cells.

rBMSC were seeded at 2×10^5 cells/mL in 6-well plates. The culture medium was replaced by MCM after culturing for 1 day. After cultured in MCM for 3 days, the expression of osteogenesis-related genes (ALP, COL-I, OCN and RUNX-2) were detected by qRT-PCR technology as mentioned in 2.5.3. The involved primer sequences are listed in Table S4.

2.9.3. Detection of p65 nuclear transportation

The inhibition of nuclear factor kappa B (NF-κB) pathway was detected by measuring the nuclear transportation of p65 which is a key downstream transcriptional factor in NF-κB pathway through an immunofluorescence assay. rBMSC were seeded at 1×10^4 cells/mL in confocal petri plates. The culture medium was replaced by MCM after culturing for 1 day. After cultured in MCM for 1 day, cells were fixed with PFA, permeabilized in 0.1 v/v% Triton X-100, blocked with 100% bovin serum albumin, and incubated with the primary antibody of anti-p65 (Abcam, ab16502) followed with fluorescent secondary antibody at 37 °C in the dark for 1 h. Cells were then stained with DAPI for 5 min, and observed using confocal laser scanning microscope (CLSM, Carl Zesis, 710 Meta, Germany).

2.10. Effects of macrophage-conditioned culture medium on HUVECs

2.11.1. Migration of HUVECs in MCM

HUVECs were seeded at 2×10^5 cells/mL in 6-well plates. When cells were reached to 90% confluence, cross lines were draw with 1 mL pipet tips. Meanwhile, the culture mediums were replaced with MCM. After culturing for another 24 h, the cells were stained with Calcein AM

(Bestbio, China) and observed in a fluorescence microscope.

2.11.2. qRT-PCR evaluation

HUVECs were seeded at 2 × 10^5 cells/mL in 6-well plates. The culture medium was replaced by MCM after culturing for 1 day. After culturing in MCM for 3 days, the expression of angiogenesis-related genes (VEGF, HIF-α and KDR) were detected by qRT-PCR technology as mentioned in 2.5.3. The involved primer sequences are listed in Table S2.

2.12. In vivo experiments

All the procedures of animal experiment were approved by the Animal Ethics Committee of Guangdong Provincial People's Hospital and applied in accordance with the Guidelines for Care and Use of Laboratory Animals of Southern Medical University.

2.13. Subcutaneous experiment

Twelve male adult Sprague–Dawley (SD) rats with body weights of ~200 g and age of 5 weeks were used. The animals were housed in clear plastic cages on clean bedding and allowed ad libitum access to water and standard laboratory fodder. Rats were intraperitoneal injected with pentobarbital sodium (40 mg/kg) to anesthetize before surgery. The bilateral back of each rat was shaved and disinfected with 2% iodine prior to the procedure. Two incisions were made on bilateral back of each rat, and each subcutaneous pocket was implanted with one sample. At 4 and 8 weeks post-procedure, the samples were harvested and the capsule tissues containing samples were also resected.

The surface morphologies of samples were observed by a scanning electron microscope (SEM, SU8220, Hitachi, Japan). The tissues harvested were fixed in 4% paraformaldehyde, dehydrated, embedded in paraffin and performed histological section. Acquired sections were stained with hematoxylin-eosin, and further imaged by a bright-field microscope (Olympus, Germany).

Furthermore, to evaluate the polarization of macrophages surrounding the implants, the above acquired sections were stained with iNOS (Invitrogen, PA1-036, green, M1 marker) and CD206 (Abcam, ab64693, red, M2 marker) according to the manufacturer's instructions. The nuclei were stained with DAPI. The stained tissues were observed by using a fluorescence microscope.

2.14. Surgery of bone implantation

Eighteen male SD rats with body weights of ~200 g and age of 5 weeks were employed to evaluate the osseointegration of the samples. The housing environment, anesthetize and disinfection method were mentioned above. Lateral approach of knee joint was selected for surgical implantation. After pre-drilling a femur medullary cavity with a 2 mm hand-operated drill, materials were implanted, and each rat implanted with one kind of sample on two femurs. Then, the wound was carefully sutured layer by layer and treated properly. All surgical protocols were conducted under aseptic conditions. Each rat was injected with prophylactic antibiotics consecutive for 3 days after surgery to avoid infection. To perform sequential fluorochromes labeling, two fluorochromes were injected intraperitoneally into the animals for group 8 weeks at 4/6 weeks post-surgery with a sequence of 30 mg/kg alizarin res S and 25 mg/kg tetracycline hydrochloride (Sigma Aldrich, USA). The rats were sacrificed by over dose injection with chloral hydrate at 4 and 8 weeks after implantation. The bilateral femoral samples were harvested for histological analysis.

2.14.1. Micro computerized tomography (micro-CT) assay

Harvested femoral samples were scanned through a high-resolution micro-CT to observe the formation of new bone and the degradation of rods. The scanning resolution is about 48 μm under 80 kV and 40 μA. The scanning matrix size was 1024 × 1024. More than 500 layers were continuously scanned at the implantation area. The bone volume percentage within a region of interest and the bone mineral density, termed BV/TV and BMD, respectively, were determined using VG Studio MAX software. The three-dimensional (3D) images of each sample were reconstructed by Multimodal 3D Visualization (Siemens, Germany) software.

2.14.2. Histological examinations and SEM observation

For histological examination, femoral/rod constructions from each group were fixed in 4% paraformaldehyde, dehydrated by gradient ethanol, and embedded in polymethylmethacrylate (PMMA).Then they were cut into thicker sections (150-200 μm) by a saw microtome (EXAKT Apparatebau, Nordestedt, Hamburg, Germany) followed with grinding and polishing into a final thickness of about 50 μm. Then the sample sections were stained with Van Gieson's (VG) solution, and the bone tissues were observed and imaged under a microscope (Olympus, Germany). The tissues were also observed by using SEM after sputtered with Pt.

2.14.3. Chronic systemic toxicity examination

In addition to bone, a patch of tissue from heart, liver, spleen, lung and kidney organs were also taken down at each time point. Then the soft tissues were fixed in 4% paraformaldehyde, dehydrated, embedded in paraffin and performed histological section. All rats were subject to blood samplings at pre-operation and every 2 weeks after operation using a vacutainer method with lithium heparin tubes from caudal vein until sacrificed. All the blood samples were centrifuged to collect the serum. The serum hematological parameters and Mg concentration were measured using a hematological auto-analyzer (Roche Hitachi 911).

2.15. Statistic analysis

All data were presented as mean ± standard deviation (SD). Statistical analysis was performed using two-way ANOVA followed by Tukey's post hoc test via SPSS 19.0 software. Statistically significant was confirmed when P-value < 0.05.

3. Results and discussions

3.1. Materials characterization and in vitro corrosion resistance

Surface morphology and element distribution of Mg, Mg-$Mg(OH)_2$ and Mg-LDH samples are shown in Fig. 1a–c, and corresponding elemental composition are shown in Fig. 1d. Scratches lines were observed on Mg surface (Fig. 1a), which was resulted from the process of ground. The surface of Mg-$Mg(OH)_2$ sample (Fig. 1b) was covered by a rough layer, which was composed with Mg and O elements. As for Mg-LDH sample (Fig. 1c) plate-like structures were detected, which was the typical morphology of LDH [34]. The element composition of plate-like structures was Mg (32.1 ± 0.1 at%), O (65.6 ± 0.4 at%) and Al (2.3 ± 0.1 at%) (Fig. 1d). Fig. S1 shows the cross-section views of Mg-$Mg(OH)_2$ and Mg-LDH, and the film thickness of the two samples were 3.67 ± 0.57 and 4.17 ± 0.07 μm, respectively. Fig. 1e shows the XRD patterns of Mg, Mg-$Mg(OH)_2$ and Mg-LDH samples. Except characteristic peaks of Mg phase, no other peaks were detected on Mg samples. For the XRD pattern of Mg-$Mg(OH)_2$ sample, feather peaks at 18.5° and 38° were detected, which represented the successful fabrication of $Mg(OH)_2$ film. In the XRD pattern of Mg-LDH sample, except peaks of $Mg(OH)_2$, a new peak at 11.7° was detected, which was the classic feature peaks of LDH structure (the face of (001)) [23]. Further considering that only Mg, Al and O element were detected on the surface of Mg-LDH, it can be concluded that the formed LDH was Mg-Al LDH.

Corrosion resistance is the first factor that should be considered for the clinic application of Mg. Fig. 2a shows the potentiodynamic

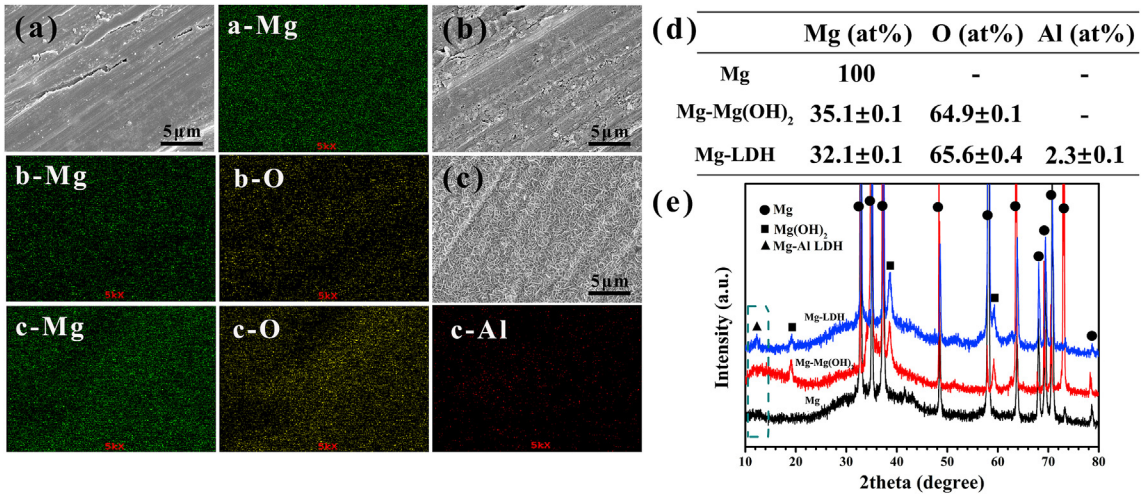

(d)	Mg (at%)	O (at%)	Al (at%)
Mg	100	-	-
Mg-Mg(OH)$_2$	35.1±0.1	64.9±0.1	-
Mg-LDH	32.1±0.1	65.6±0.4	2.3±0.1

Fig. 1. Surface views and corresponding element distribution of Mg (a), Mg-Mg(OH)$_2$ (b) and Mg-LDH (c). Element composition (d) and XRD patterns (e) of Mg, Mg-Mg(OH)$_2$ and Mg-LDH.

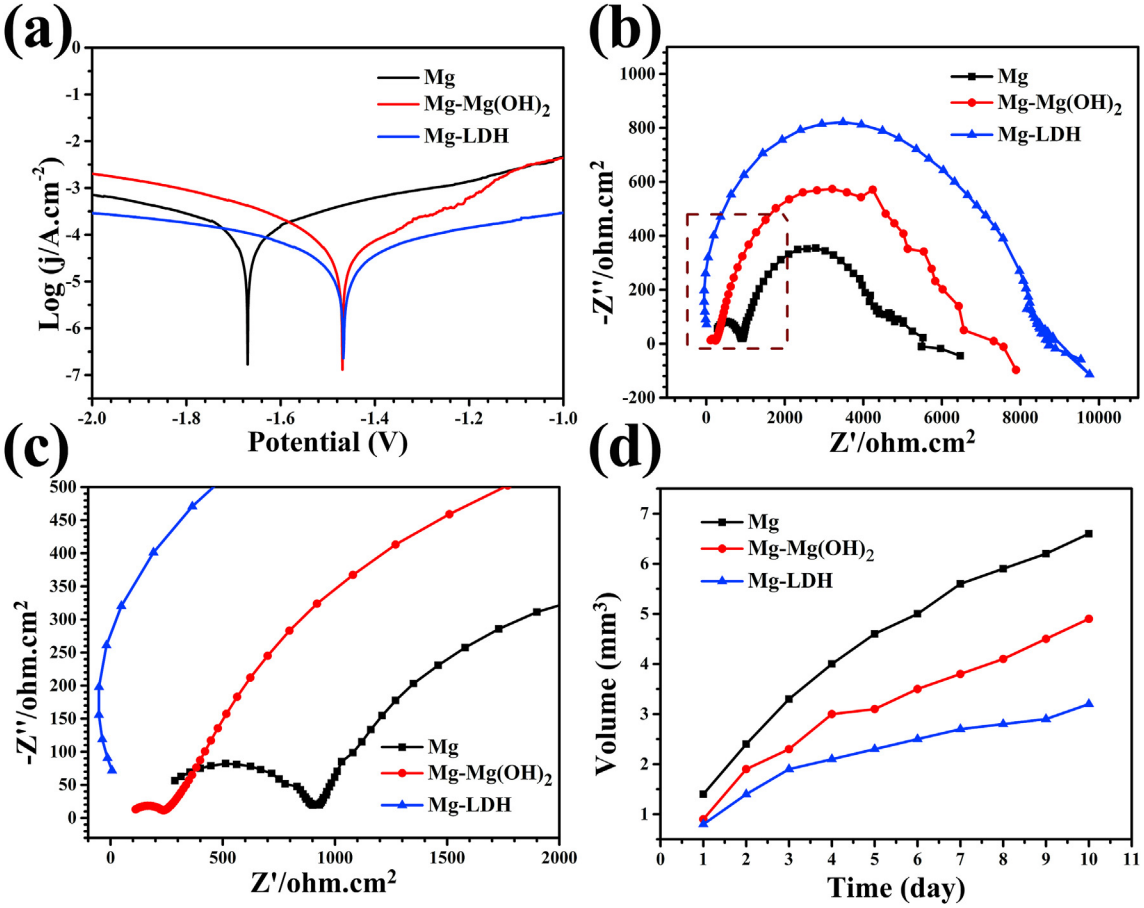

Fig. 2. Potentiodynamic polarization (a) and EIS (b) resuts of Mg, Mg-Mg(OH)$_2$, Mg-LDH. The magnification of the block in (b) shown in (c). Accumulative hydrogen evolution of various samples after immersed in PBS (d).

Table 1
Corrosion data of Mg, Mg-Mg(OH)$_2$, Mg-LDH samples.

	E_{corr} (V)	j_{corr} (A/cm^2)	R_p (Ω cm^2)	R_{ct} (Ω cm^2)
Mg	−1.67	8×10^{-5}	1.3×10^4	1149
Mg-Mg(OH)$_2$	−1.48	3.4×10^{-5}	3.6×10^4	1740
Mg-LDH	−1.46	1.62×10^{-5}	6.66×10^4	2386

polarization curves of Mg, Mg-Mg(OH)$_2$ and Mg-LDH. The calculated corrosion parameters are shown in Table 1. Compared with Mg sample, both Mg-Mg(OH)$_2$ and Mg-LDH samples exhibited significantly higher corrosion potential (E_{corr}) and lower free current density (j_{corr}), especially for Mg-LDH sample. The polarization resistance (R_p) of Mg-Mg(OH)$_2$ and Mg-LDH samples were 2.77 and 5.12 times that of Mg sample. It can be easily concluded that Mg-LDH showed best corrosion resistance. EIS was also applied to evaluate the electrochemical

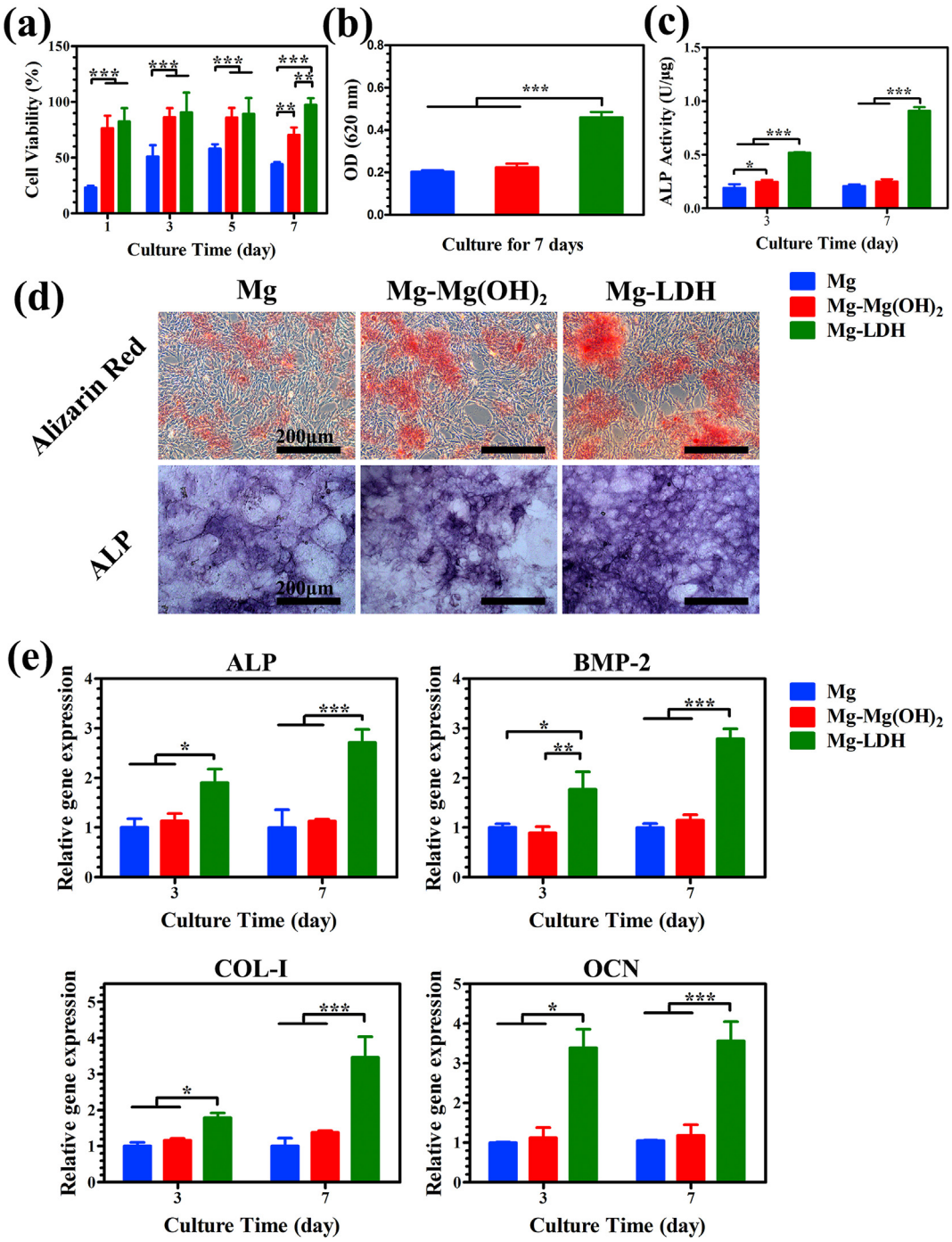

Fig. 3. Cell viability of MC3T3-E1 cultured in the extracts for 1, 3, 5 and 7 days (a). Quantitative results of matrix mineralization (b) and ALP activity (c) of MC3T3-E1, and corresponding staining area (d). Expression of osteogenesis-related genes of MC3T3-E1 cultured in the extracts (e).

corrosion of the three samples and the results are shown in Fig. 2b and c. Mg-LDH sample displayed largest impedance and followed by Mg-Mg $(OH)_2$ and Mg samples. The equivalent electrical circuit model of the EIS results can be fitted as R_s (Q_f (R_f (Q_{dl} R_{ct}))) (Fig. S2) [35,36], among which R_{ct} means the charge transfer resistance of the electrical double layer. It is well known that R_{ct} refers to the impedance of the corrosion reaction and the fitted results are shown in Table 1. The R_{ct} values of Mg-$Mg(OH)_2$ and Mg-LDH samples are 1.5 and 2 time of Mg sample, respectively, indicating the best corrosion protection of Mg-LDH film. The EIS results are consistence with the results of potentiodynamic polarization cure.

According to the reaction of $Mg + H_2O \rightarrow Mg^{2+} + OH^- + H_2$ (gas), the release of hydrogen can reflect the corrosion rate of Mg substrate. The hydrogen evolution results are displayed in Fig. 2d. The hydrogen release of Mg sample was obvious suppressed after hydrothermal treated and Mg-LDH sample exhibited slowest hydrogen evolution. This result proved again that Mg-LDH film can provide better corrosion protection than Mg-$Mg(OH)_2$ film.

In our previous work, better corrosion resistance of Mg-Al LDH film than $Mg(OH)_2$ film on JDBM magnesium alloy was already proved [23]. The enhanced corrosion resistance of Mg-Al LDH film could be ascribed to its anion exchange ability, which can protect the film from the attack of Cl^-. In the present study, we further prove that Mg-Al LDH film can work on pure Mg substrate.

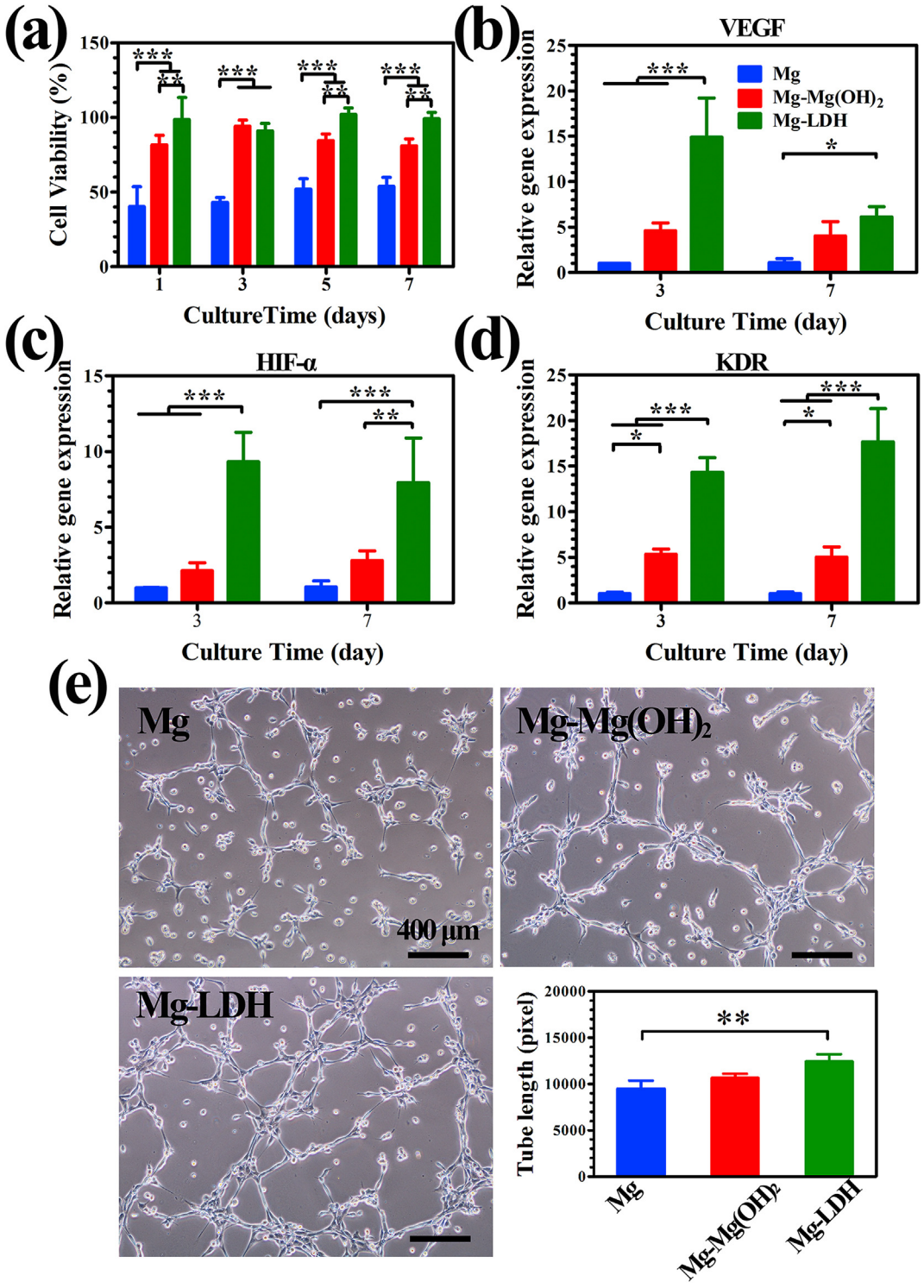

Fig. 4. Cell viability of HUVECs cultured in the extracts for 1, 3, 5 and 7 days (a). Expression of angiogenesis-related genes of HUVEs cultured in the extracts: (b) VEGF, (c) HIF-α and (d) KDR. *In vitro* angiogenesis of HUVECs cultured with various extracts on ECMatrix gel and corresponding tube lengths (e).

3.2. *In vitro* osteogenesis ability and angiogenic behavior

Cell viability of different extracts towards MC3T3-E1 was studied by CCK-8 assay to evaluate the cytocompatibility, and the results are shown in Fig. 3a. Cell viability of cells in the extract of Mg group was about 50% at day 1–7, indicating severe cytotoxicity. However, extract of Mg-$Mg(OH)_2$ and Mg-LDH samples exhibited significantly higher cell proliferation (≥80%), indicating slight cytotoxicity. Moreover, Mg-LDH group showed best cell viability at day 7, which may suitable for long term implantation. In addition, for the early adhesion of MC3T3-E1, more lamellipodia extensions was found on MC3T3-E1 cultured in the extract of Mg-LDH for 24 h than cultured in Mg and Mg-$Mg(OH)_2$ groups (Fig. S3). Our previous study revealed that cell viability decreased significantly when concentration of Mg^{2+} higher than 20 mM or pH value higher than 8.5 [37]. The extract of pure Mg would experience a severe change of Mg^{2+} concentration and pH value, thus leading to a severe cytotoxicity. After modification, the corrosion resistance of Mg-$Mg(OH)_2$ and Mg-LDH samples enhanced and thus their

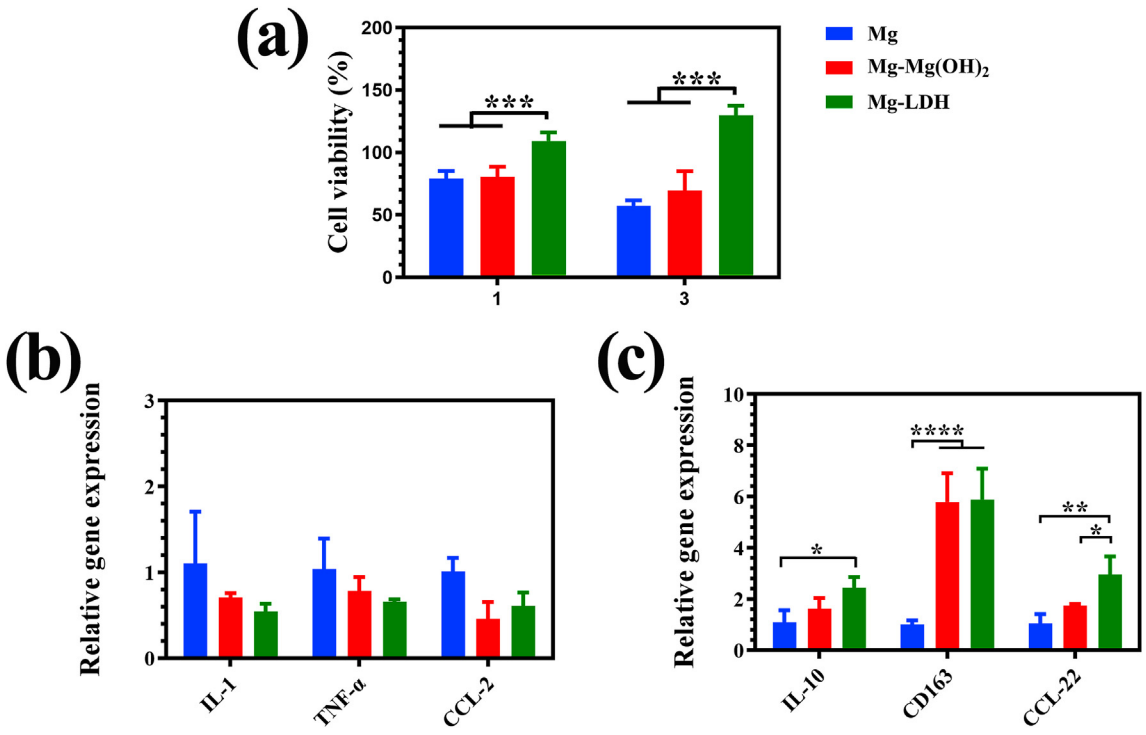

Fig. 5. Cell viability of RAW cultured in the extracts for 1 and 3 days (a). Expression of M1-related (b) and M2-related (c) genes of RAW264.7 cultured in the extracts for 3 days.

extracts showed better compatibility, especially for Mg-LDH sample (cell viability higher than 95% at all times). It should be noted that Al has long been reported to alter blood-brain barrier and had an adverse impact on the central nervous system. The European Food Safety Authority (EFSA) suggested that the tolerable daily intake of Al by a 60-kg adult is 17.1 mg [38]. However, Al^{3+} was not detected in Mg-LDH extract using inductively coupled plasma optical emission spectrometry (ICP-OES) with a lowest detectable limitation of 0.5 μg/Ml, suggesting that content in Mg-LDH sample is too low to cause damage to the body.

ECM and ALP activity are the important signs of osteogenic differentiation. ECM was evaluated by Alizarin red staining and the results are represented in Fig. 3b and d. It can be seen that Mg coated with LDH film significantly improved the red staining area. The relative absorbance value of the matrix mineralization in Mg, Mg-$Mg(OH)_2$ and Mg-LDH group were 0.2 ± 0.01, 0.2 ± 0.02 and 0.5 ± 0.03 respectively, which further indicated the best ECM ability of Mg-LDH sample. Results of ALP activity are shown in Fig. 3c and d. Quantitative assay showed an increased ALP activity in Mg-LDH and Mg-$Mg(OH)_2$ group at day 3, while the Mg-LDH group presented highest ALP activity. At day 7, both qualitative and quantitative results indicate that Mg-LDH sample remained highest ALP activity. The influence of extracts on osteogenic differentiation of MC3T3-E1 was further investigated on the molecular level. The expression of osteogenesis-related genes such as ALP, BMP-2, Col-I and OCN, were evaluated by RT-PCR. BMP-2 is a potent growth factor involved in regulating bone formation; Col-I is one of the most abundant extracellular matrixes of bone; OCN is a kind of non-collagenous glycoproteins secreted by osteoblast during bone formation. As shown in Fig. 3e, the expression of the four genes were similar in the extracts of Mg and Mg-$Mg(OH)_2$ samples, while significantly higher in the extract of Mg-LDH sample, both at day 3 and day 7. All the results mentioned above confirm that Mg-LDH sample possessed the strongest osteogenic induce ability than Mg and Mg-Mg $(OH)_2$ samples.

Though MC3T3-E1 in the extract of Mg-$Mg(OH)_2$ sample showed better cell adhesion and cell viability than in that of Mg sample, its osteogenic differentiation level was equal to Mg sample. The results suggested that Mg^{2+} concentration and pH value had different impact on cell viability and differentiation, which the other researchers should pay attention for. Nevertheless, for Mg-LDH sample, its extract was not only suitable for cell adhesion and proliferation, but also favorable for osteogenic differentiation.

As main source of nutrients such as oxygen, hormones and growth factors delivered to nourishing bone cells, vasculature is indispensable for appropriate bone remodeling. HUVECs is the most important cell which participates in vessel formation. Fig. 4a displays cell viability of HUVECs after cultured in various extracts. The cell viability of HUVECs showed the same trend as the cell viability (Fig. 3a) of MC3T3-E1 cultured in various extract, and the extract of Mg-LDH sample was most suitable for HUVECs proliferation. To investigate the angiogenic effect of various extracts on gene level, angiogenic-associated genes including KDR, VEGF and HIF-α were detected by RT-PCR after being cultured for 3 and 7 days, and the results are depicted in Fig. 4b–d. The transcription level of HIF-α (Fig. 4c) and KDR (Fig. 4d) were significantly up-regulated in Mg-LDH group compared to other groups at each time point. At day 3, the expression of VEGF of Mg-LDH group was significantly higher than the other two samples. However, at day 7, no significantly difference of VEGF expression was observed between Mg-LDH and Mg-$Mg(OH)_2$ samples, but the former was still obviously higher than that of Mg sample. Collectively, LDH film on Mg can improve the expression of angiogenic-associated genes. Tube formation is a classic method to test HUVECs differentiation tendency *in vitro*. As shown in Fig. 4e, the total branches length in Mg, Mg-$Mg(OH)_2$ and Mg-LDH groups were 9490 ± 869.2, 10662 ± 432.7 and 12419 ± 778.2 pixel respectively, which suggest that more HUVECs were connected to form vessel like structures in Mg-LDH group. All the above data indicated that Mg-LDH sample was more suitable for the angiogenic behavior of HUVECs.

With best corrosion resistance, the extract of Mg-LDH sample would experience a slightest change of pH value and Mg^{2+} concentration compare to Mg and Mg-$Mg(OH)_2$ samples. In this case, favorable pH value and Mg^{2+} concentration leaded to its favorable *in vitro* vascularization and osteogenic differentiation abilities.

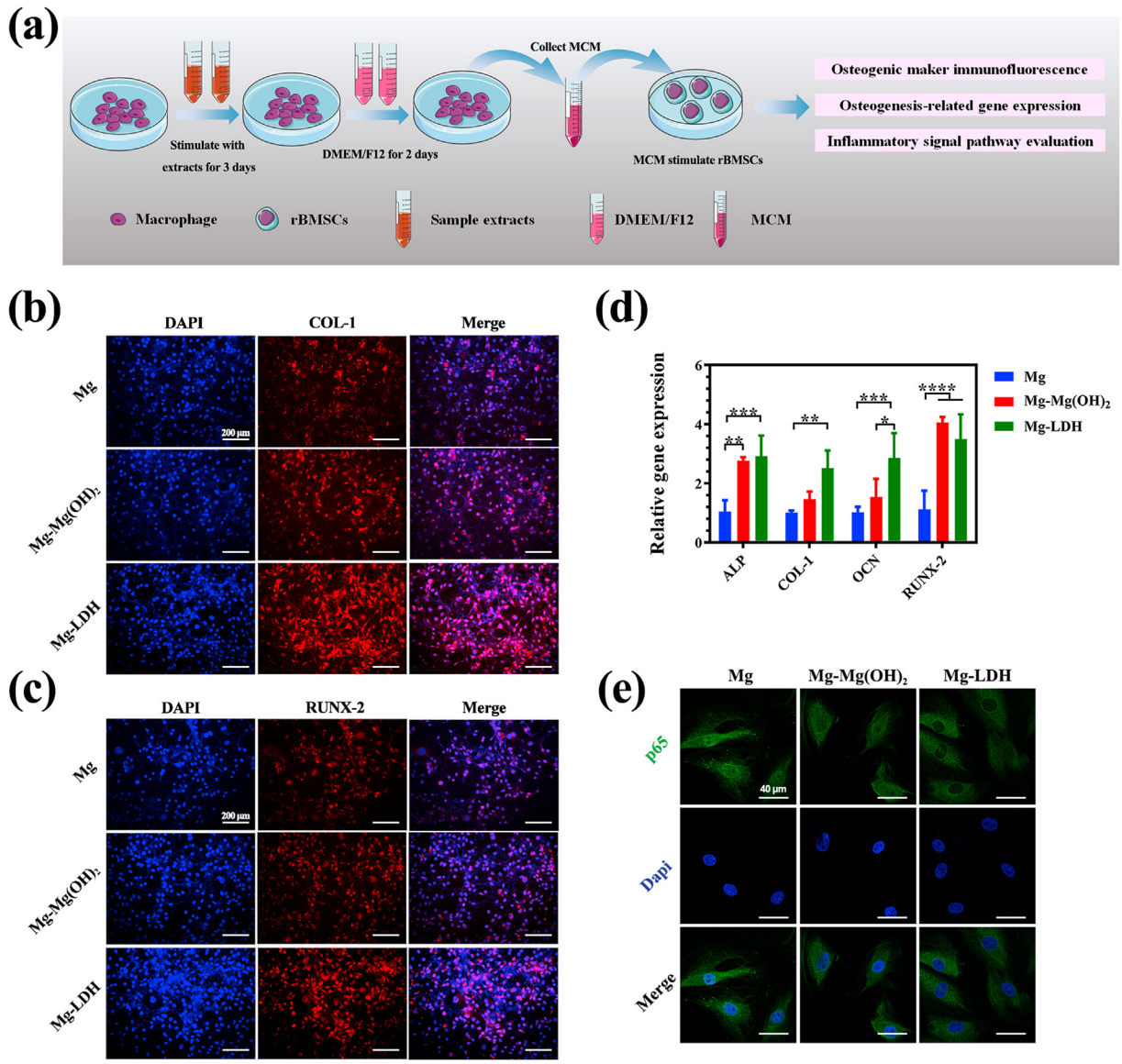

Fig. 6. The illustration of experimental design (a). Immunofluorescence staining of COL-I (b) and RUNX (c) on rBMSCs after being activated by MCM. Osteogenesis-related genes expression of rBMSCs after being activated by MCM (d). Immunofluorescence staining of p65 to evaluate the inhibition of NF-κB pathway (e).

3.3. In vitro immune response

Once biomaterial is implanted *in vivo*, macrophages will response to the implants immediately, and thus determining the behavior of osteogenesis-related cells, including rBMSCs and HUVECs. Fig. 5a shows the cell viability of RAW264.7 cultured in various extracts. It can be seen that cells' proliferation was suppressed in the extracts of Mg and Mg-Mg(OH)$_2$ groups. However, in the extract of Mg-LDH, cell viability was a slightly higher than 100% at day 1, and further increased to approximately 130% at day 3. This result is consistent with the cell viability of MC3T3-E1 (Fig. 3a) and HUVECs (Fig. 4a), that is Mg and Mg-Mg(OH)$_2$ extracts were toxicity, while the extract of Mg-LDH was relatively safety. The M1-and M2-related genes expression of RAW264.7 are displayed Fig. 5b and c, respectively. For M1-related genes, although a lowest gene expression of IL-1 and TNF-α can be seen in cells cultured in Mg-LDH extracts, but there was no significant difference among three detected groups on the expression of IL-1, TNF-α and CCL-2 genes. For M2-related genes, cells cultured in the extract of Mg-LDH exhibited a higher expression of CCL-22 than that of Mg and Mg-Mg(OH)$_2$ groups. Although no significant different was observed in the expression of IL-10 and CD163 between the extracts of Mg-Mg(OH)$_2$ and Mg-LDH, but the expression of these two genes of cells cultured in Mg-LDH was significantly higher than that in bare Mg groups. Taking all the detected eight genes in the consideration, we can conclude that Mg-LDH group was more favorable for RAW264.7 polarize to M2 phenotype.

To further investigate the influence of RAW264.7 in osteogenesis-related cells, we used MCM to culture rBMSCs (Fig. 6a). Fig. 6b and c shows the expression of COL-I and RUNX proteins on rBMSCs after being cultured in various MCM, respectively. It can be seen that fluorescence intensity of COL-I and RUNX-2 was stronger in the Mg-LDH group than the other two groups. At molecular level (Fig. 6d), rBMSCs cultured in MCM of Mg-LDH group exhibited highest expression of COL-I and OCN. The expression of ALP and RUNX-2 genes were in a same level when cultured in MCM of Mg-LDH and Mg-Mg(OH)$_2$ group, but higher than in Mg group. Both the results of immunofluorescence staining and qRT-PCR revealed that anti-inflammatory cytokines and growth factors secreted by RAW264.7 after activated by Mg-LDH extracts was more benefit for the osteogenic differentiation of rBMSCs than the other two groups.

NF-κB family transcription factors are master regulator of immune and inflammatory process [39]. Once the macrophage polarizing to M1

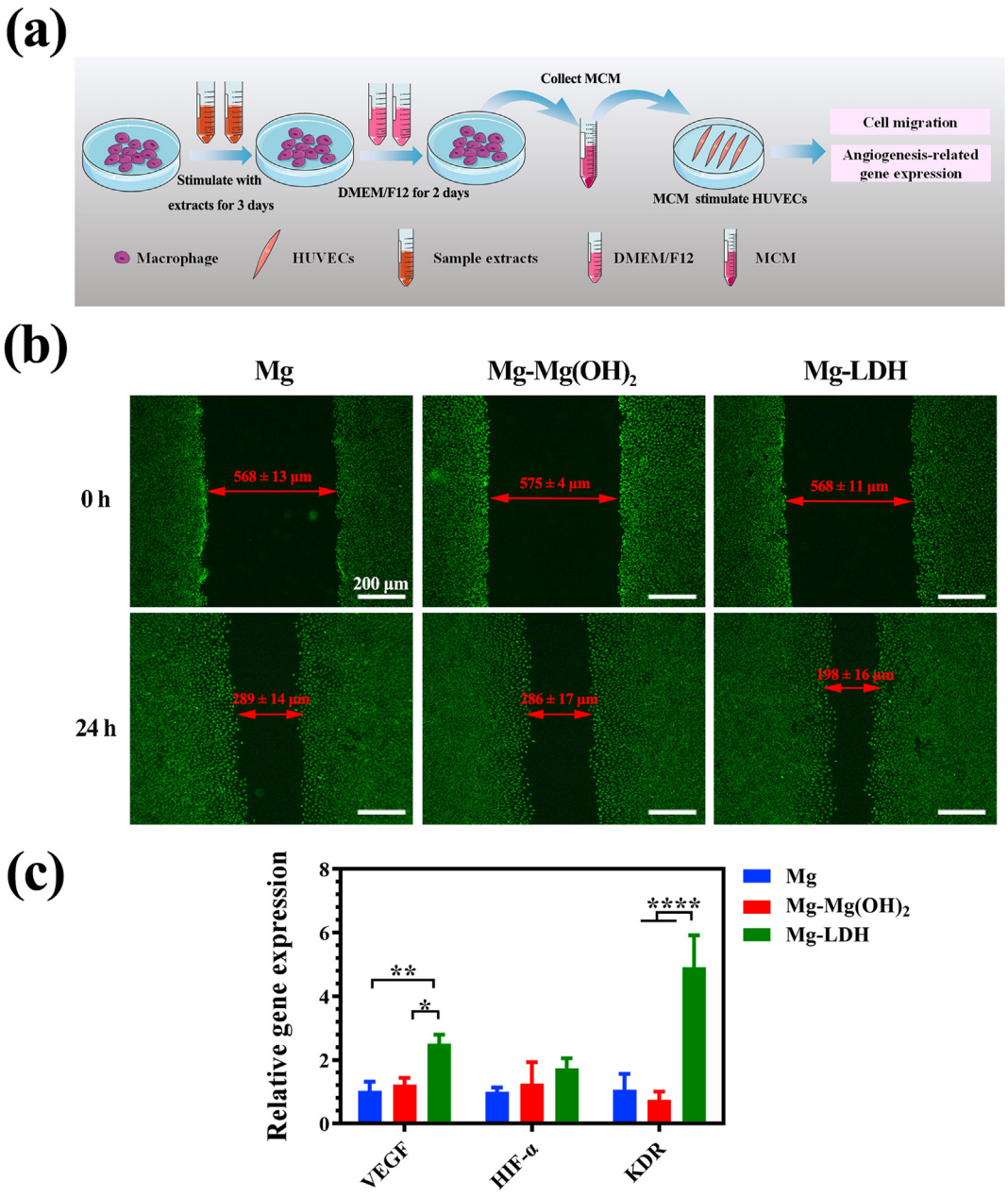

Fig. 7. The illustration of experimental design (a). Migration (b) and angiogenesis-related gene expression (b) of HUVECs after being cultured in MCM.

phenotype, it will secret a large number of inflammation cytokines, such as TNF-α and IL-1. These cytokines will activate NF-κB signaling pathway and inhibit the osteogenic differentiation of rBSMCs [40–42]. p65 play a central role in NF-κB signaling pathway by entering nuclear and activating downstream genes [39]. The staining of p65 and nucleus of rBSMCs cultured in various MCM is presented in Fig. 6e. Strongest green dye could be observed in the site of nucleus of Mg group, followed by Mg-Mg(OH)$_2$ group. For Mg-LDH group, almost no fluorescence was observed in the nucleus site. The above data suggested that after coated Mg with Mg-Al LDH, the sample can significantly suppress macrophage activating to M1 phenotype, and thus suppressing the activation of NF-κB signaling pathway. Once NF-κB signaling pathway was inhibited, rBSMCs would experience an enhanced osteogenic differentiation.

The influence of MCM on the migration and angiogenesis-related gene expression of HUVECs were studied (Fig. 7a) and the results are displayed in Fig. 7b and 7c respectively. It can be seen from Fig. 7b that the gaps of all the groups were narrower after 24 h cultivation compared with the initial scratched gaps. More detailed, the gap of HUVECs cultured in MCM of Mg-LDH group was narrowest among the three groups, indicating its fastest migration. For the expression of angiogenesis-related genes, HUVECs cultured in Mg-LDH group exhibited a highest expression of VEGF and KDR genes. It should be noted that no significant difference was observed in the expression of HIF-α among the three groups. In all, both the result of cell migration and gene expression suggested that macrophage activated by Mg-LDH extract is more favorable for the angiogenic behavior of HUVECs.

Nevertheless, the *in vitro* microenvironment is huge different from the *in vivo,* thus it is also vital to investigate the corrosion resistance, inflammation response and osteointergation of Mg-Al LDH coated Mg *via* animal experiments.

3.4. Subcutaneous implantation

Subcutaneous implantation test was used to evaluate the corrosion resistance, histocompatibility and immune response of Mg, Mg-Mg

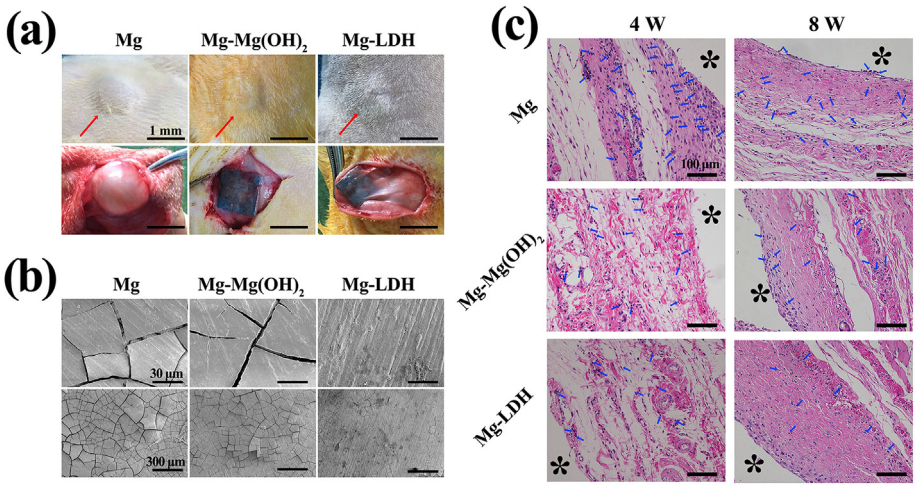

Fig. 8. Optical photograph of subcutaneous capsules (a) and SEM views (b) of Mg, Mg-$Mg(OH)_2$, Mg-LDH after implantation for 4 weeks. Photomicrographs of histological section of Mg, Mg-$Mg(OH)_2$, Mg-LDH after implantation for 4 and 8 weeks. The red asterisk represented the sample and blue arrow indicated neutrophils.

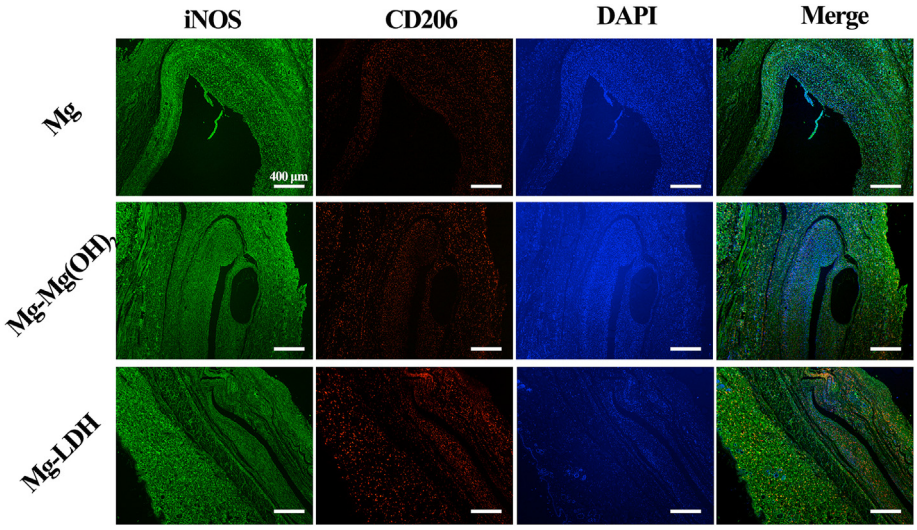

Fig. 9. Immunofluorescent staining of the tissue surrounding the implants after subcutaneous implantation for 8 weeks.

$(OH)_2$ and Mg-LDH. The skin and subcutaneous tissue surrounding the materials after implanted 4 weeks were pictured and are displayed in Fig. 8a. It can be seen that an obviously bubble appeared around Mg implant, which was consistent with the *in vitro* hydrogen evolution test (Fig. 2d). No gas accumulated around Mg-$Mg(OH)_2$ and Mg-LDH implants. Because the $Mg(OH)_2$ and LDH films can significantly reduce the degradation of Mg substrate, thus fewer hydrogen would release from the implanted materials, and the released gas can be absorbed by the host healing ability [1]. Furthermore, the implanted samples were scanned by SEM (Fig. 8b). Obvious cracks can be observed on the surface of Mg and Mg-$Mg(OH)_2$ samples, and especially for Mg. However, almost no cracks were detected on the surface of Mg-LDH sample, which suggested that Mg-Al LDH film can resist the attack of body fluid and thus protect Mg substrate from degradation. Both the optical pictures and micrographs prove that Mg-LDH film can also work *in vivo*. It should be noted that the cracks were observed at Mg-LDH sample after implanted for 8 weeks (Fig. S4), implying the reduce protection ability of Mg-Al LDH film. The subcutaneous tissues attaching to the samples were collected and stained with H&E staining, and the results are shown in Fig. 8c. It can be observed that all samples can induce local tissue inflammation at 4 weeks, and then became milder at 8 weeks. Fewest neutrophils (indicated by blue arrows) were observed on the tissue around Mg-LDH sample, indicating its mildest inflammation. Though *in vitro* and *in vivo* environment is different, the results of subcutaneous implantation prove that Mg-LDH sample also showed favorable corrosion resistance and histocompatibility *in vivo*.

Fig. 9 shows the immunofluorescence images of iNOS and CD206. It can be seen that the fluorescence intensity of iNOS of the three groups were similar to each other, but a significantly stronger expression of CD206 was observed for Mg-LDH group. In the merge images, a stronger red fluorescence was presented in Mg-LDH group, indicating its higher proportion of M2 macrophages. This result was consistent with the result of H&E staining, and both the results suggest that Mg-LDH sample would induce milder inflammatory microenvironment after implanted *in vivo*, compared with bare Mg and Mg-$Mg(OH)_2$ samples.

3.5. Femoral implantation

To visually display degradation trend of Mg, Mg-$Mg(OH)_2$ and Mg-LDH samples, sectional views of micro-CT imaging at 4 and 8 weeks after implantation are displayed in Fig. 10a. At week 4, the corrosion depth on Mg-LDH sample was obvious smaller than that on Mg and Mg-$Mg(OH)_2$ samples. At week 8, Mg-LDH sample still showed the best completeness with less area of pitting corrosion (indicated by red arrow). This result suggested that Mg-LDH showed best corrosion

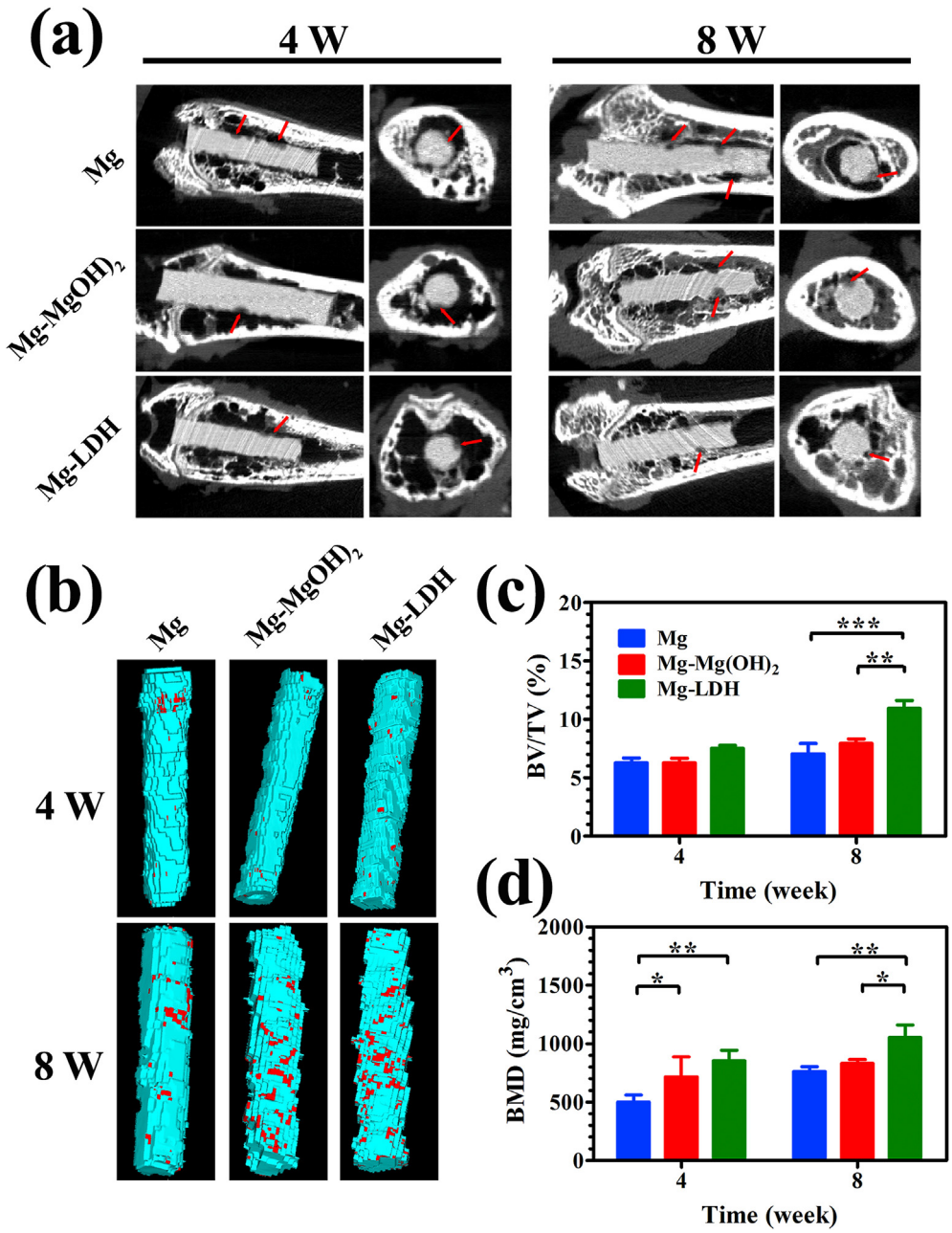

Fig. 10. Micro-CT analysis of Mg, Mg-Mg(OH)$_2$, Mg-LDH after implantation for 4 and 8 weeks (a), representative horizontal and vertical sections are shown, red arrows indicate the degradation position. Corresponding three-dimensional reconstruction images of Micro-CT results (b), red sections indicate new bone. Calculated bone volume/tissue volume (BV/TV) (c) and trabecular bone mineral density (BMD) (d).

resistance in bone, which was consistent with the result of *in vitro* corrosion and subcutaneous implantation tests. Fig. 10b represents the 3D-reconstructed of Micro-CT images. On all the implants, few new bones (marked in red) were formed at week 4. As the implantation time extension to 8 weeks, more new bone were observed on all the implants, especially for Mg-Mg(OH)$_2$ and Mg-LDH samples. Figs. 10c and d displays the calculated results of BV/TV and BMD, respectively. At week 4, no significant difference between the BV/TV value of the three samples, but the BMD value of Mg-Mg(OH)$_2$ and Mg-LDH samples were significantly higher than the that of Mg. At week 8, both the BV/TV and BMD of Mg-LDH was highest, indicting its best bone formation.

Fig. 11a and b exhibit the histological stained images of bone-implant interface. For all implants, cancellous bone (indicated by blue arrows) grew into the peri-implant gaps at week 4. However, the newly formed cancellous bone was closer to the implant for Mg-LDH than the other two samples. At week 8, the formed bone was still not connected with the implant for Mg and Mg-Mg(OH)$_2$ samples. However, for Mg-LDH implant, it can be found that newly formed bone was closely connected with the implant in some sites (indicated by yellow ellipse). These results indicate that Mg-LDH sample exhibited better osseointegration than Mg and Mg-Mg(OH)$_2$ samples. Fig. 11c shows the SEM images corresponding to VG staining. At high magnification, corrosion layer was observed on all implants. At low magnification, pure Mg implant experienced a most serious corrosion. More new bones (indicated by yellow square) surrounding the Mg-LDH implant than the other two groups. Meanwhile, the newly formed bone surrounding the Mg-LDH implant was closer to the implant than the other two groups, indicating a best osteointegration of Mg-LDH sample. These results further confirmed by the sequential fluorescent labeling (Fig. S5). All these observations were consistent with the results of VG staining.

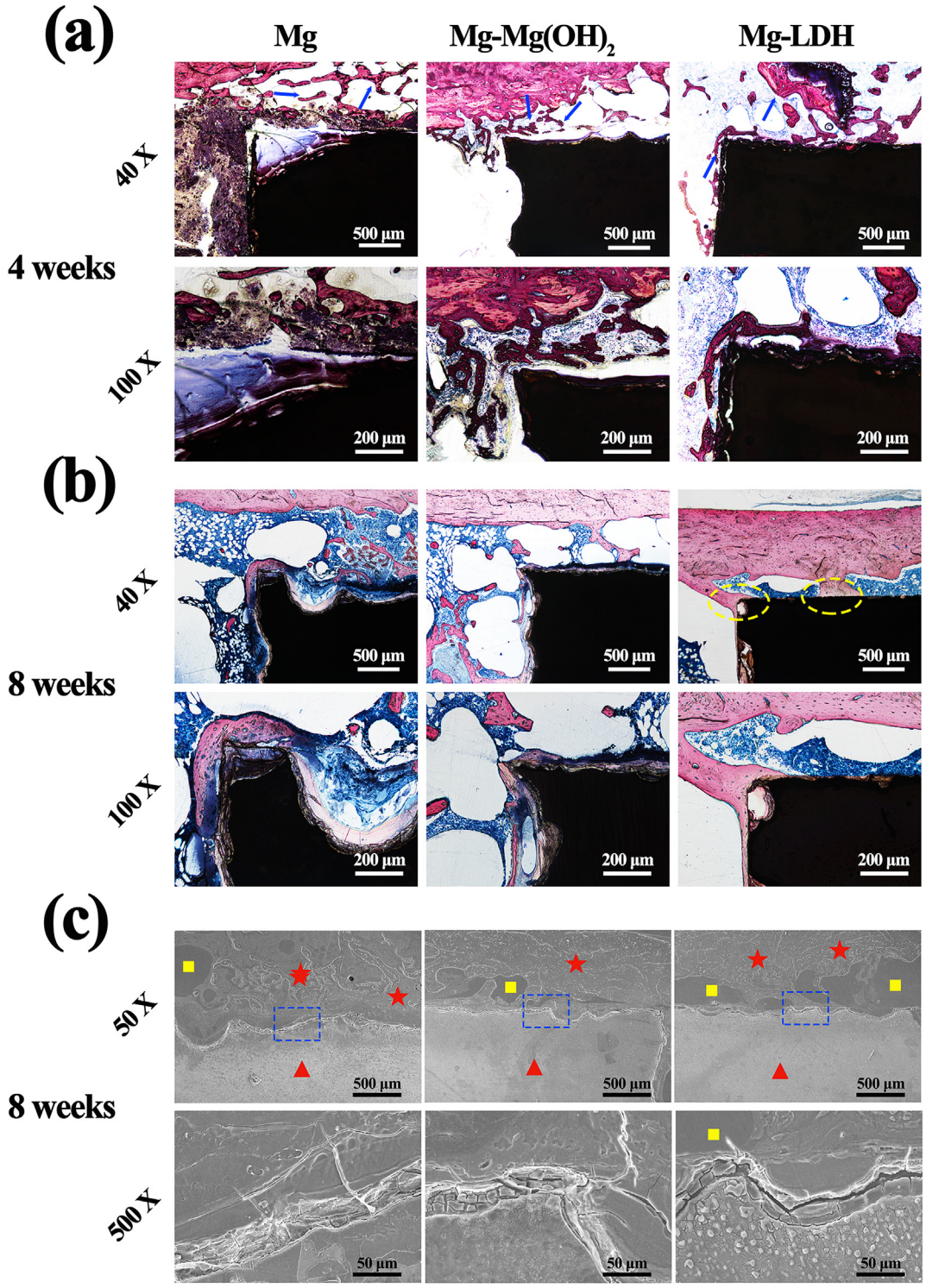

Fig. 11. VG staining of Mg, Mg-$Mg(OH)_2$ and Mg-LDH samples after femur implantation for 4 weeks (a) and 8 weeks (b). Blue arrow indicates formed cancellous bone, yellow ellipses indicate well osseointegration section. SEM observations of Mg, Mg-$Mg(OH)_2$ and Mg-LDH samples after femur implanted for 8 weeks (c). Red triangles indicate the implant, red asterisks indicate the PMMA, yellow squares indicate the new bone.

The degradation products of Mg based implants would influence the surrounding microenvironment [43], and thus then influence the bone formation process. Though proper Mg^{2+} is good for osteogenic differentiation and proper OH^- is benefit for inorganic salt (such as hydroxyapatite) deposition on implant, but an excessive concentration of Mg^{2+} and OH^-, accompanied with massive hydrogen, would release from bare Mg substrate [8,9,44], resulting in its poor bone regeneration. Both $Mg(OH)_2$ and Mg-Al LDH films can improve the corrosion resistance, and the latter show better protection of Mg substrate. Therefore, Mg-LDH implant showed more moderate degradation, thus more suitable for bone regeneration and osseointergation. In addition, the *in vitro* results of cell culture revealed that Mg-LDH sample was more favorable more the osteogenic differentiation of MC3T3-E1 and the angiogenic behavior of HUVECs, as well as induced better immune response for osteogenesis and angiogenesis. All these factors discussed above lead to a better osteointegration of Mg-LDH implant.

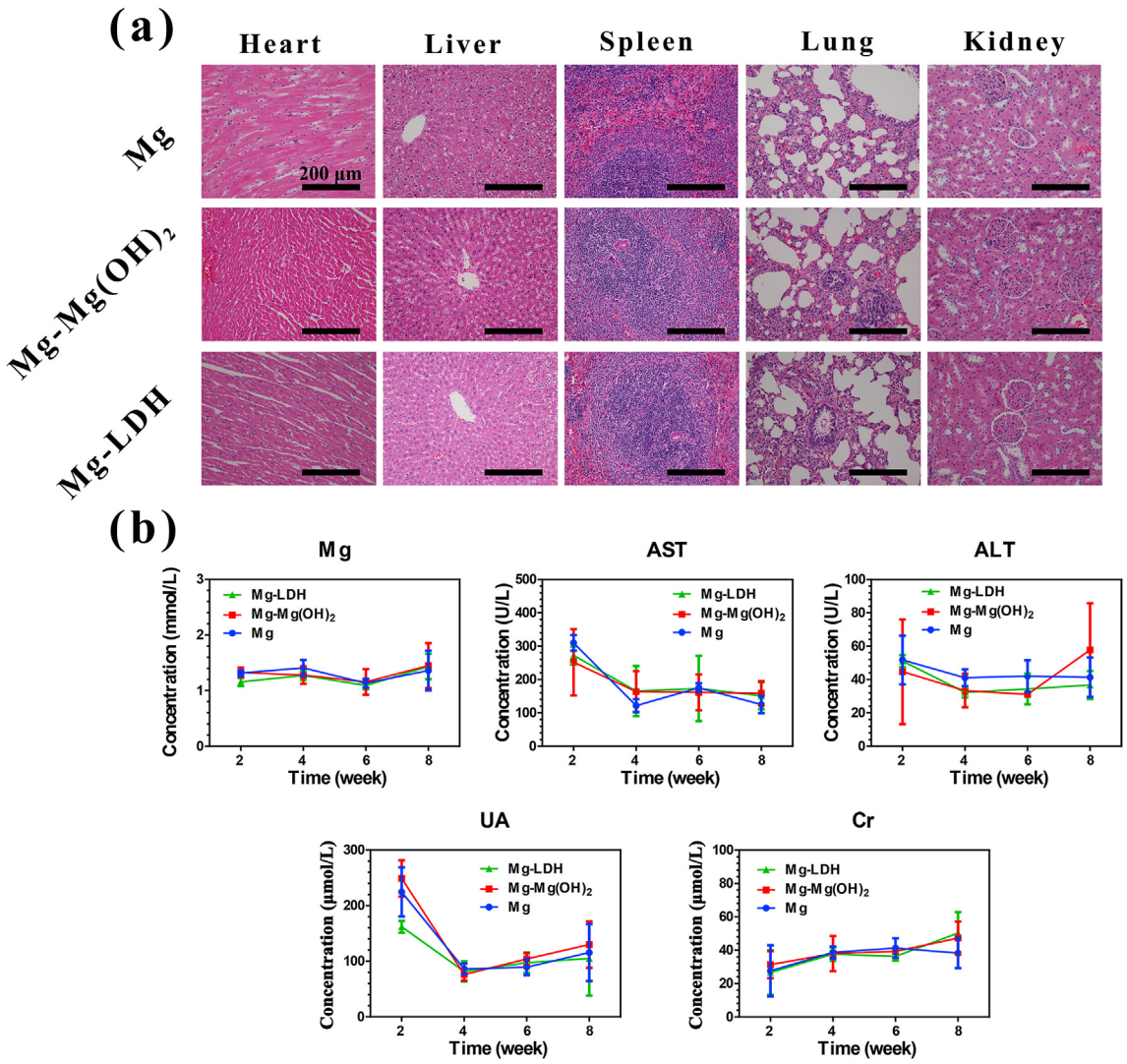

Fig. 12. Typical histological morphology of important organic tissues in H&E sections of Mg, Mg-$Mg(OH)_2$, Mg-LDH samples after femur implantation for 8 weeks (a). Level of main serum indices: Mg, aspartate aminotransferase (AST), alanine aminotransferase (ALT), uric acid (UA), creatinine (Cr) (b).

Biosafety is another vital issue should be concerned for implants. For Mg based implants, the degradation products (such as Mg^{2+}, OH^- and hydrogen) would circulate to the bloodstream, and then influence organic tissues [45]. The H&E staining of important tissues were applied. No obvious pathological changes were observed in heart, liver, spleen, lung and kidney after implantation for 4 weeks (Fig. S6) and 8 weeks (Fig. 12a). Fig. 12b exhibits the changes of blood indices after femoral implantation. The trends were similar for all the samples. In details, the concentration of Mg, alanine aminotransferase (ALT) and creatinine (Cr) were relatively stable at all time points. Though the concentration of aspartate aminotransferase (AST) and uric acid (UA) was slightly high at week 2, but quickly return to normal at week 4. The above results confirmed that Mg and modified Mg implants in this study are biosafety.

4. Conclusion

In this work, Mg-Al LDH coating was fabricated on pure Mg via hydrothermal treatment. Compared with bare Mg and $Mg(OH)_2$ coated Mg, Mg-Al LDH coated sample showed better *in vitro* and *in vivo* corrosion resistance. *In vitro* cell culture experiments revealed that Mg-Al LDH coated sample was more suitable for the osteogenic differentiation of MC3T3-E1 and vascularization of HUVECs. Meanwhile, Mg-LDH coated Mg was more favorable for macrophages polarize to M2 phenotype, and then inhibited the activation of NF-κB signaling pathway on rBMSCs. The proper immune response was benefit for the osteogenesis and angiogenesis behaviors. In addition, the results of femoral implantation indicated that Mg-Al LDH film on Mg would enhance bone regeneration and osseointegration. With systematic investigation of the response of osteogenesis-related and angiogenesis-related cells to LDH coating, as well as the immune response of LDH coating *via in vitro* and *in vivo* experiments. This study proves that Mg-Al LDH has a potential application as protection coating on Mg for orthopedic applications.

CRediT authorship contribution statement

Shi Cheng: Supervision, Project administration, Data curation, Conceptualization, Investigation, Methodology, Data curation. **Dongdong Zhang:** Supervision, Project administration, Data curation. **Mei Li:** Supervision, Project administration, Data curation. **Xuanyong Liu:** Project administration, Investigation. **Yu Zhang:** Project administration, Investigation, Supervision, Funding acquisition, Writing - review & editing. **Shi Qian:** Supervision, Funding acquisition, Writing - review & editing. **Feng Peng:** Conceptualization, Investigation, Methodology, Data curation, Supervision, Funding acquisition, Writing - review & editing.

Declaration of competing interest

The authors declare no conflict of interest.

Acknowledgements

Financial supported from the China Postdoctoral Science Foundation (2019M662830), National Natural Science Foundation of China (31771044), Shanghai Committee of Science and Technology, China (18410760600), International Partnership Program of Chinese Academy of Sciences Grant No. GJHZ1850, Natural Science Foundation of Guangdong Province, China (Grant No. 2020A1515011447), and Scientific and Technological Projects of Guangzhou, China (Grant No. 202002030283).

Appendix A. Supplementary data

Supplementary data to this article can be found online at https://doi.org/10.1016/j.bioactmat.2020.07.014.

References

[1] D. Zhao, F. Witte, F. Lu, J. Wang, J. Li, L. Qin, Current status on clinical applications of magnesium-based orthopaedic implants: a review from clinical translational perspective, Biomaterials 112 (2017) 287–302.
[2] M. Ali, M.A. Hussein, N. Al-Aqeeli, Magnesium-based composites and alloys for medical applications: a review of mechanical and corrosion properties, J. Alloys Compd. 792 (2019) 1162–1190.
[3] S. Kamrani, C. Fleck, Biodegradable magnesium alloys as temporary orthopaedic implants: a review, Biometals 32 (2019) 185–193.
[4] H. Windhagen, K. Radtke, A. Weizbauer, J. Diekmann, Y. Noll, U. Kreimeyer, R. Schavan, C. Stukenborg-Colsman, H. Waizy, Biodegradable magnesium-based screw clinically equivalent to titanium screw in hallux valgus surgery: short term results of the first prospective, randomized, controlled clinical pilot study, Biomed. Eng. Online 12 (2013).
[5] J.W. Lee, H.S. Han, K.J. Han, J. Park, H. Jeon, M.R. Ok, H.K. Seok, J.P. Ahn, K.E. Lee, D.H. Lee, S.J. Yang, S.Y. Cho, P.R. Cha, H. Kwon, T.H. Nam, J.H. Lo Han, H.J. Rho, K.S. Lee, Y.C. Kim, D. Mantovani, Long-term clinical study and multiscale analysis of in vivo biodegradation mechanism of Mg alloy, Proc. Natl. Acad. Sci. U.S.A. 113 (2016) 716–721.
[6] G.Y. Yuan, J.L. Niu, Research progress of biodegradable magnesium alloys for orthopedic applications, Acta Metall. Sin. 53 (2017) 1168–1180.
[7] S. Chen, L. Tan, B. Zhang, Y. Xia, K. Xu, K. Yang, In Vivo study on degradation behavior and histologic response of pure magnesium in muscles, J. Mater. Sci. Technol. 33 (2017) 469–474.
[8] Y. Yu, H. Lu, J. Sun, Long-term in vivo evolution of high-purity Mg screw degradation - local and systemic effects of Mg degradation products, Acta Biomater. 71 (2018) 215–224.
[9] P. Han, P. Cheng, S. Zhang, C. Zhao, J. Ni, Y. Zhang, W. Zhong, P. Hou, X. Zhang, Y. Zheng, Y. Chai, In vitro and in vivo studies on the degradation of high-purity Mg (99.99wt.%) screw with femoral intracondylar fractured rabbit model, Biomaterials 64 (2015) 57–69.
[10] K. Chen, X.H. Xie, H.Y. Tang, H. Sun, L. Qin, Y.F. Zheng, X.N. Gu, Y.B. Fan, In vitro and in vivo degradation behavior of Mg-2Sr-Ca and Mg-2Sr-Zn alloys, Bioactive Materials 5 (2020) 275–285.
[11] P.F. Ding, Y.C. Liu, X.H. He, D.B. Liu, M.F. Ghen, In vitro and in vivo biocompatibility of Mg-Zn-Ca alloy operative clip, Bioactive Materials 4 (2019) 236–244.
[12] X.B. Chen, C.Q. Li, D.K. Xu, Biodegradation of Mg-14Li alloy in simulated body fluid: a proof-of-concept study, Bioactive Materials 3 (2018) 110–117.
[13] Y.F. Zheng, X.N. Gu, F. Witte, Biodegradable metals, Mater. Sci. Eng. R Rep. 77 (2014) 1–34.
[14] P. Tian, X. Liu, Surface modification of biodegradable magnesium and its alloys for biomedical applications, Regen Biomater 2 (2015) 135–151.
[15] M. Echeverry-Rendon, J.P. Allain, S.M. Robledo, F. Echeverria, M.C. Harmsen, Coatings for biodegradable magnesium-based supports for therapy of vascular disease: a general view, Materials Science & Engineering C-Materials for Biological Applications 102 (2019) 150–163.
[16] S. Agarwal, J. Curtin, B. Duffy, S. Jaiswal, Biodegradable magnesium alloys for orthopaedic applications: a review on corrosion, biocompatibility and surface modifications, Mater Sci Eng C Mater Biol Appl 68 (2016) 948–963.
[17] Z. Lin, Y. Zhao, P.K. Chu, L. Wang, H. Pan, Y. Zheng, S. Wu, X. Liu, K.M.C. Cheung, T. Wong, K.W.K. Yeung, A functionalized TiO2/Mg2TiO4 nano-layer on biodegradable magnesium implant enables superior bone-implant integration and bacterial disinfection, Biomaterials 219 (2019) 119372.
[18] Z.Q. Zhang, L. Wang, M.Q. Zeng, R.C. Zeng, M.B. Kannan, C.G. Lin, Y.F. Zheng, Biodegradation behavior of micro-arc oxidation coating on magnesium alloy-from a protein perspective, Bioactive Materials 5 (2020) 398–409.
[19] L. Guo, W. Wu, Y. Zhou, F. Zhang, R. Zeng, J. Zeng, Layered double hydroxide coatings on magnesium alloys: a review, J. Mater. Sci. Technol. 34 (9) (2018) 1455–1466.
[20] C.Y. Li, L. Gao, X.L. Fan, R.C. Zeng, D.C. Chen, K.Q. Zhi, In vitro degradation and cytocompatibility of a low temperature in-situ grown self-healing Mg-Al LDH coating on MAO-coated magnesium alloy AZ31, Bioactive Materials 5 (2020) 364–376.
[21] K. Zhang, Q. Feng, J. Xu, X. Xu, F. Tian, K.W.K. Yeung, L. Bian, Self-assembled injectable nanocomposite hydrogels stabilized by bisphosphonate-magnesium (Mg2+) coordination regulates the differentiation of encapsulated stem cells via dual crosslinking, Adv. Funct. Mater. 27 (2017) 1701642.
[22] M.Q. Zhao, Q. Zhang, J.Q. Huang, F. Wei, Hierarchical nanocomposites derived from nanocarbons and layered double hydroxides - properties, synthesis, and applications, Adv. Funct. Mater. 22 (2012) 675–694.
[23] F. Peng, H. Li, D. Wang, P. Tian, Y. Tian, G. Yuan, D. Xu, X. Liu, Enhanced corrosion resistance and biocompatibility of magnesium alloy by Mg-Al-layered double hydroxide, ACS Appl. Mater. Interfaces 8 (2016) 35033–35044.
[24] N. Kamiyama, G. Panomsuwan, E. Yamamoto, T. Sudare, N. Saito, T. Ishizaki, Effect of treatment time in the Mg(OH)2/Mg–Al LDH composite film formed on Mg alloy AZ31 by steam coating on the corrosion resistance, Surf. Coating. Technol. 286 (2016) 172–177.
[25] G. Zhang, L. Wu, A. Tang, S. Zhang, B. Yuan, Z. Zheng, F. Pan, A novel approach to fabricate protective layered double hydroxide films on the surface of anodized Mg-Al alloy, Advanced Materials Interfaces 4 (2017) 1700163.
[26] A.P. Kusumbe, S.K. Ramasamy, R.H. Adams, Coupling of angiogenesis and osteogenesis by a specific vessel subtype in bone, Nature 507 (2014) 323.
[27] C.J. Percival, J.T. Richtsmeier, Angiogenesis and intramembranous osteogenesis, Dev. Dynam. 242 (2013) 909–922.
[28] W. Katagiri, T. Kawai, M. Osugi, Y. Sugimura-Wakayama, K. Sakaguchi, T. Kojima, T. Kobayashi, Angiogenesis in newly regenerated bone by secretomes of human mesenchymal stem cells, Maxillofac Plast Reconstr Surg 39 (2017) 8.
[29] R. Sridharan, A.R. Cameron, D.J. Kelly, C.J. Kearney, F.J. O'Brien, Biomaterial based modulation of macrophage polarization: a review and suggested design principles, Mater. Today 18 (2015) 313–325.
[30] Q.R. Wang, Z.Q. He, M.G. Huang, T.R. Liu, Y.L. Wang, H.N. Xu, H. Duan, P.H. Ma, L. Zhang, S.S. Zamvil, J. Hidalgo, Z.F. Zhang, D.M. O'Rourke, N. Dahmane, S. Brem, Y.G. Mou, Y.Q. Gong, Y. Fan, Vascular niche IL-6 induces alternative macrophage activation in glioblastoma through HIF-2 alpha, Nat. Commun. 9 (2018).
[31] A.L. Ponte, E. Marais, N. Gallay, A. Langonne, B. Delorme, O. Herault, P. Charbord, J. Domenech, The in vitro migration capacity of human bone marrow mesenchymal stem cells: comparison of chemokine and growth factor chemotactic activities, Stem Cell. 25 (2007) 1737–1745.
[32] H. Li, F. Peng, D. Wang, Y. Qiao, D. Xu, X. Liu, Layered double hydroxide/polydopamine composite coating with surface heparinization on Mg alloys: improved anticorrosion, endothelialization and hemocompatibility, Biomater Sci 6 (2018) 1846–1858.
[33] L. Zhang, J. Pei, H. Wang, Y. Shi, J. Niu, F. Yuan, H. Huang, H. Zhang, G. Yuan, Facile preparation of poly(lactic acid)/brushite bilayer coating on biodegradable magnesium alloys with multiple functionalities for orthopedic application, ACS Appl. Mater. Interfaces 9 (2017) 9437–9448.
[34] F. Peng, D. Wang, D. Zhang, B. Yan, H. Cao, Y. Qiao, X. Liu, PEO/Mg–Zn–Al LDH composite coating on Mg alloy as a Zn/Mg ion-release platform with multifunctions: enhanced corrosion resistance, osteogenic, and antibacterial activities, ACS Biomater. Sci. Eng. 4 (2018) 4112–4121.
[35] L. Zhang, E.A.A. Mohammed, A. Adriaens, Synthesis and electrochemical behavior of a magnesium fluoride-polydopamine-stearic acid composite coating on AZ31 magnesium alloy, Surf. Coating. Technol. 307 (2016) 56–64.
[36] Z. Wei, P. Tian, X. Liu, B. Zhou, In vitro degradation, hemolysis, and cytocompatibility of PEO/PLLA composite coating on biodegradable AZ31 alloy, J. Biomed. Mater. Res. B Appl. Biomater. 103 (2015) 342–354.
[37] F. Peng, D.H. Wang, Y.X. Tian, H.L. Cao, Y.Q. Qiao, X.Y. Liu, Sealing the pores of PEO coating with Mg-Al layered double hydroxide: enhanced corrosion resistance, cytocompatibility and Drug delivery ability, Sci. Rep. 7 (2017).
[38] K. Klotz, W. Weistenhofer, F. Neff, A. Hartwig, C. van Thriel, H. Drexler, The health effects of aluminum exposure, Dtsch Arztebl Int 114 (2017) 653–659.
[39] N.J.W. H, Molecular basis of NF-κB signaling, Annu. Rev. Biophys. 42 (2013) 443–468.
[40] W. Y, L. Y, Z. M, L. L, Z. X, Z. P, Z. Y, Inhibition of PTGS1 promotes osteogenic differentiation of adipose-derived stem cells by suppressing NF-kB signaling, Stem Cell Res. Ther. 10 (2019) 57.
[41] L. S, Z. M, L. J, H. B, J. D, H. H, S. J, LIPUS inhibited the expression of inflammatory factors and promoted the osteogenic differentiation capacity of hPDLCs by inhibiting the NF-κB signaling pathway, J. Periodontal. Res. 55 (2020) 125–140.
[42] C. J, Y. M, L. X, S. Qf, Y. Cz, Y. Ps, Progranulin promotes osteogenic differentiation of human periodontal ligament stem cells via tumor necrosis factor receptors to inhibit TNF-α sensitized NF-kB and activate ERK/JNK signaling, J. Periodontal. Res. 55 (3) (2019) 363–373.
[43] Y.S. Wang, X. Li, M.F. Chen, Y. Zhao, C. You, Y.K. Li, G.R. Chen, In Vitro and in vivo degradation behavior and biocompatibility evaluation of microarc oxidation-fluoridated hydroxyapatite-coated Mg-Zn-Zr-Sr alloy for bone application, ACS Biomater. Sci. Eng. 5 (2019) 2858–2876.
[44] M. Razavi, Y. Huang, Assessment of magnesium-based biomaterials: from bench to clinic, Biomaterials Science 7 (2019) 2241–2263.
[45] D. Zhao, T. Wang, K. Nahan, X. Guo, Z. Zhang, Z. Dong, S. Chen, D.T. Chou, D. Hong, P.N. Kumta, W.R. Heineman, In vivo characterization of magnesium alloy biodegradation using electrochemical H2 monitoring, ICP-MS, and XPS, Acta Biomater. 50 (2017) 556–565.